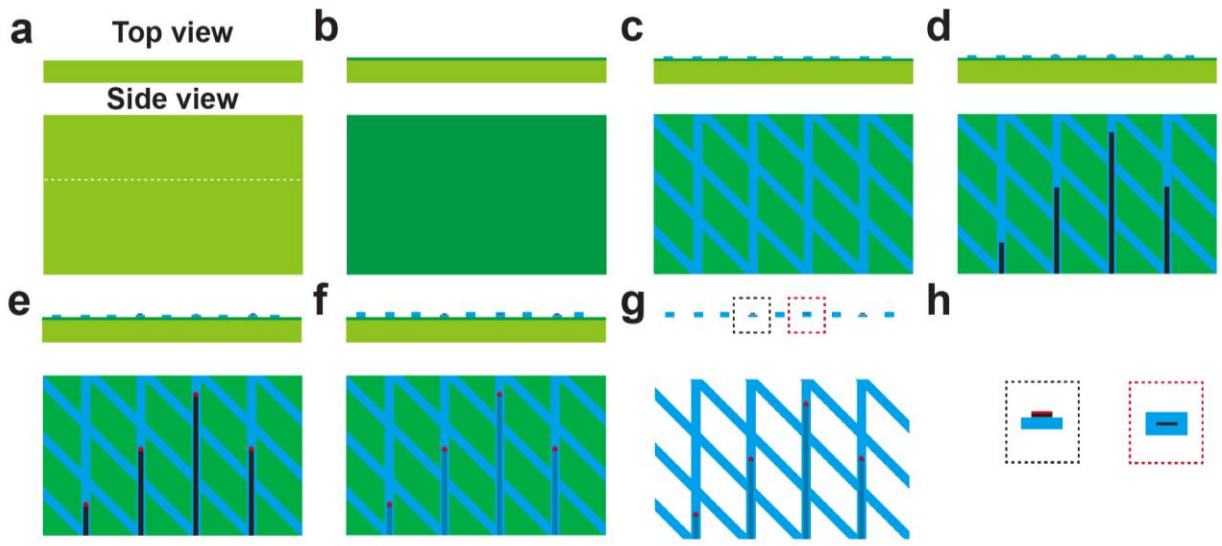

Supplementary Figure 1

Schematic steps of mesh electronics fabrication.

Components include silicon wafer (light green), nickel relief layer (dark green), polymer ribbons (blue), metal interconnects (black) and exposed metal electrodes (red). For each step (**a**-**g**) both top and side views are shown, where the side view corresponds to a cross-section taken at the position indicated by the white horizontal dashed line in the top view image of (**a**). (**h**) Zoomed-in views of regions highlighted by black (exposed Pt electrodes) and red dashed boxes (fully passivated interconnects) in (**g**).

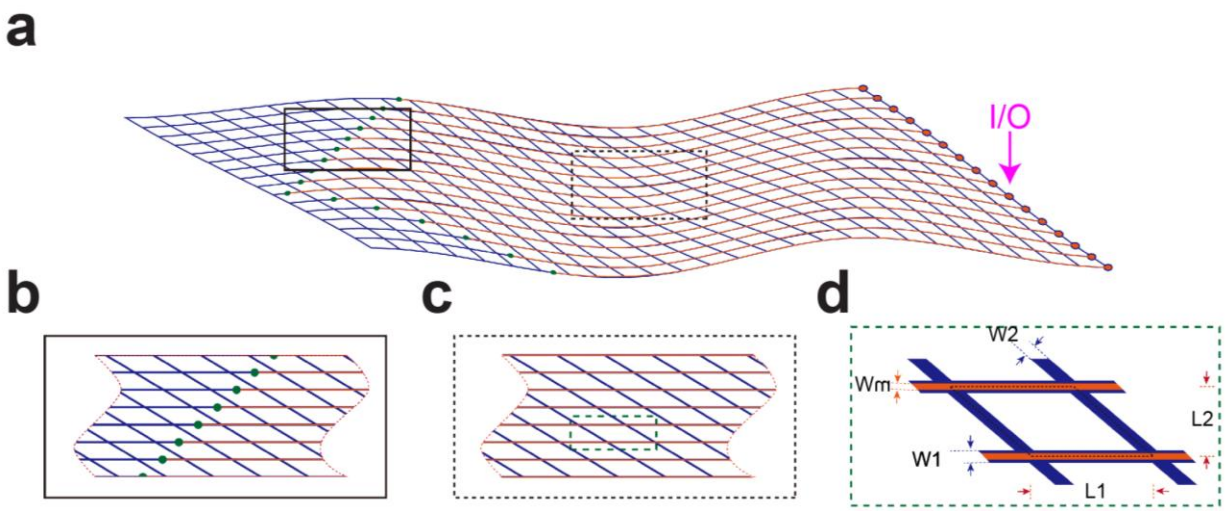

Supplementary Figure 2

Schematic structure of mesh electronics.

(**a**) Schematic of the injectable mesh electronics. Blue lines highlight the overall mesh structure and indicate the regions of supporting and passivating polymer layers, the ~horizontal orange lines indicate Au metal interconnects between input/output (I/O) pads (orange filled circles, indicated by the magenta arrow) and Pt recording electrodes (green filled circles), respectively. The solid-line black box at left highlights several of the recording electrodes, and the dashed-line black box in the middle highlights several of the metal interconnects of the mesh electronics. (**b**) A zoomed-in view of the recording electrodes highlighted by solid-line black box in (**a**). (**c**) A zoomed-in view of the mesh electronics highlighted by dashed-line black box in (**a**). (**d**) A zoomed-in view of a unit cell of the mesh (dashed-line green box in (**c**)) with the same color codes as in (**a, c**). Polymer ribbons (blue) with and without metal interconnects (orange) correspond to longitudinal and transverse elements, respectively. L1 and L2 show spacing between longitudinal and spacing between transverse elements, respectively; W1 and W2 are widths of the longitudinal and transverse mesh elements, respectively; and Wm is the width of metal interconnect lines.

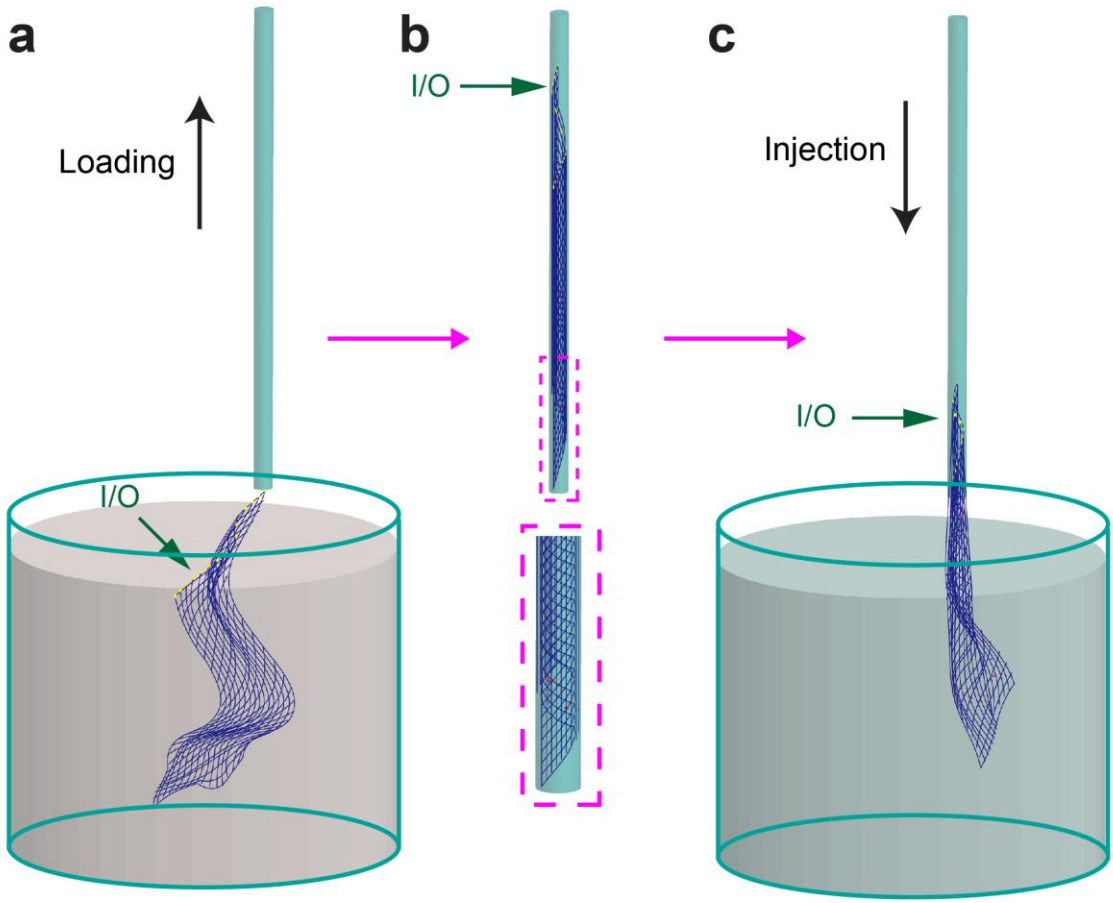

Supplementary Figure 3

Schematics illustrating method used to load the mesh electronics into a glass capillary needle and subsequently inject into a medium.

(**a**) The injectable mesh electronics (dark blue) suspended in solution (light pink) was drawn into the glass needle such that the I/O pads (yellow dots, indicated by green arrows) of the mesh enter the tube first. (**b**) After the mesh electronics was fully loaded into the glass needle with mesh end at needle tip (magenta dashed box), the needle was removed from the solution. (**c**) The glass needle was mounted in an x-y-z manipulator for injection into solution, gel/polymer or tissue (light blue). Black arrows indicate the direction of the fluid flow during loading and injection.

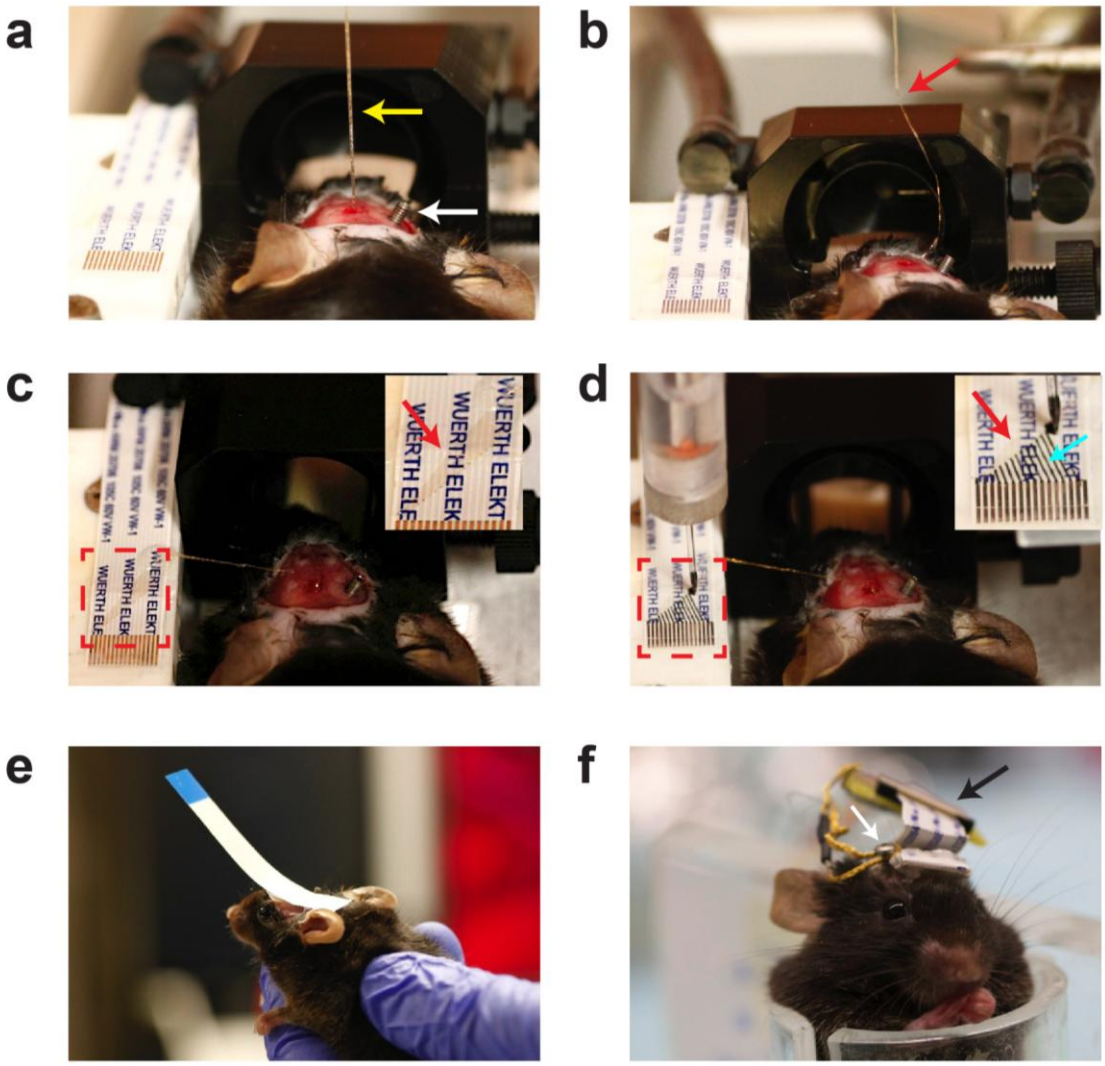

Supplementary Figure 4

Mesh electronics injection and chronic recording from mouse brain.

(**a**) Image of a mouse fixed in a stereotaxic frame with scalp skin retracted, and a hole drilled through the skull plate. The glass needle (yellow arrow) loaded with mesh electronics is visible directly above the skull in this image. A flexible flat cable (FFC) is visible at the left of the image supported on a ceramic scaffold. A 0-80 grounding screw (white arrow) was positioned at the posterior side of the skull. (**b**) Image showing the relocation of the I/O end of the post-injected mesh electronics (red arrow) towards the FFC. (**c**) Image post-injection into the brain showing the input/output (I/O) region of the mesh electronics unfolded onto the FFC. Inset shows a zoom-in view of the red dashed box, which highlights the unfolded I/O part (red arrow) of the injected mesh electronics. (**d**) Image representing the unfolded I/O pads of the mesh electronics which were electrically-connected to the FFC using the conductive ink printing process described in ref. 33. The red dashed box highlighted by the inset shows the details of the bonding with the red and cyan arrows indicating the mesh electronics and conductive ink connections, respectively. (**e**) Image showing the FFC fixed on top of the mouse skull using dental cement. (**f**) Image of a fully awake but restrained mouse during chronic *in vivo* brain recording. The white and black arrows highlight the grounding screw and the connector between FFC and external recording setups, respectively. See Online Methods for all experimental details of surgery and injection. The width of FFC in all panels is ~8 mm.

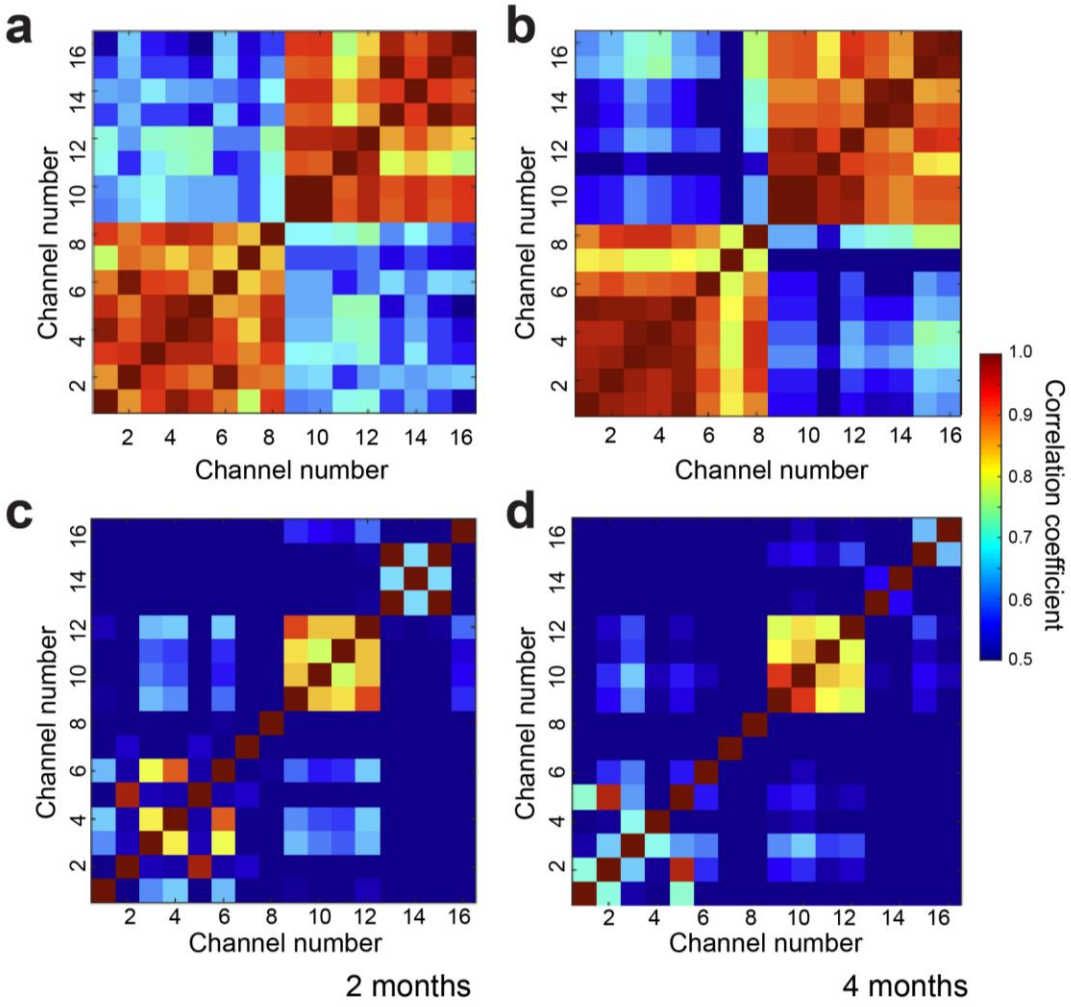

Supplementary Figure 5

Correlation maps of chronic multiplexed brain recording.

(**a**,**b**) Correlation maps of 16-channel local field potential (LFP) recordings at two (**a**) and four (**b**) months post-injection. (**c**,**d**) Correlation maps of 16-channel extracellular action potential recordings at two (**c**) and four (**d**) months post-injection. Colors indicate the correlation coefficient between any two given channels according to the color bar shown on the far right. All the maps were calculated from 2 s long data traces at both time points. See Online Methods for details of correlation coefficient calculations.

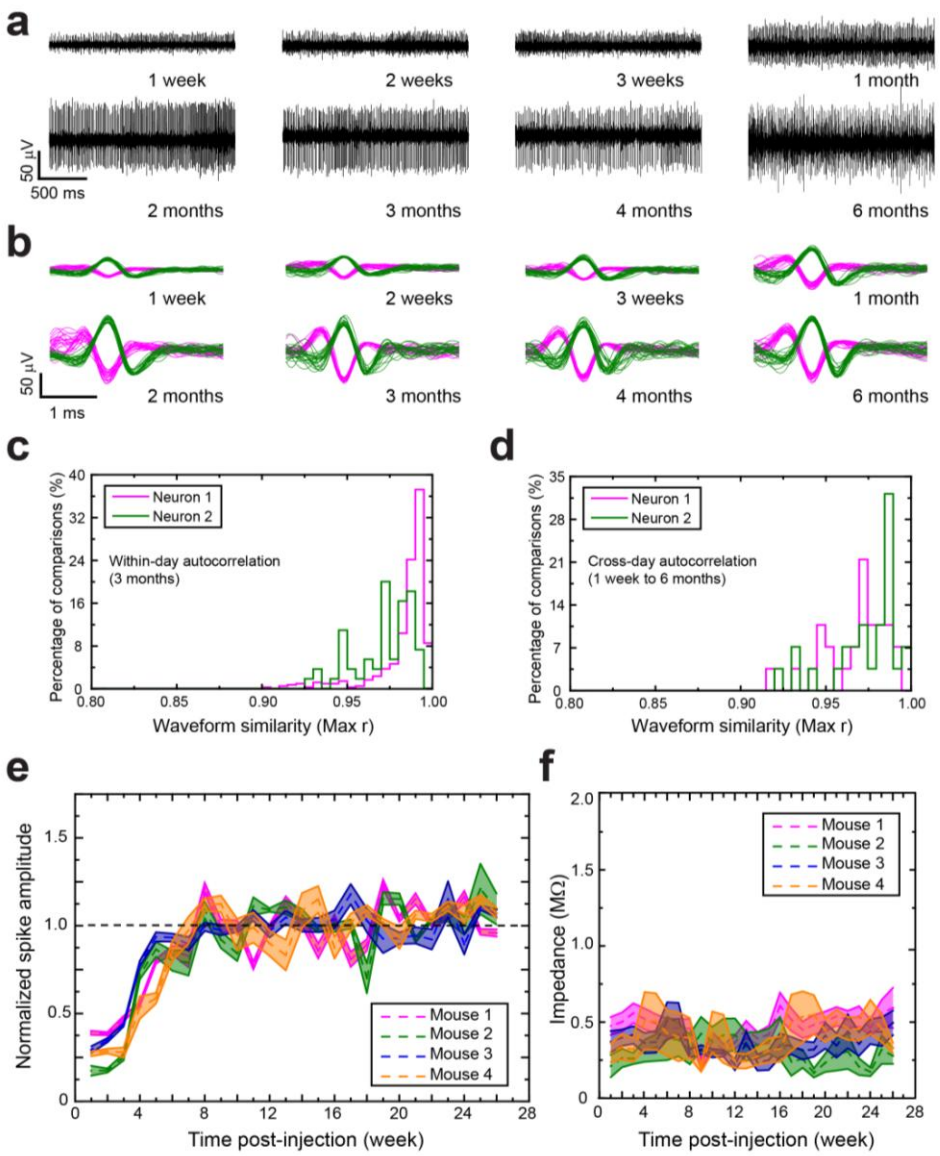

Supplementary Figure 6

Long-term stable recording without signal degradation over six months.

(**a**) Representative extracellular action potential recordings from the same electrode (Mouse4-ChannelA shown in **Fig. 2b**) located in somatosensory cortex (CTX) at different time points post-injection. (**b**) Spike sorting results of the corresponding recordings shown in (**a**). All of the spikes from the corresponding time points in (**a**) are included with ca. 50 spikes at each point. (**c**) Autocorrelation histograms of average waveforms of sorted spikes from 30 1-min segments within a 30-min recording session for Mouse4-ChannelA at 3 months post-injection. (**d**) Autocorrelation histograms of average waveforms for each of the two identified clusters (color coded in magenta (neuron 1) and green (neuron 2)) for Mouse4-ChannelA at the 8 time points shown in (**b**). See Online Methods for details of waveform autocorrelation calculations. (**e**) Time evolution of normalized average peak-to-peak spike amplitudes across all channels with single-unit action potentials recorded (the average was done across 14, 5, 6 and 7 channels for Mouse 1 to 4, respectively) from four mice. The spike amplitude was normalized (value=1.0, gray dashed horizontal lines) against the average peak-to-peak amplitude values between 5 to 26 weeks post-injection for each channel. (**f**) Average impedance values at 1 kHz across all channels with recorded single-unit action potentials of the four mice shown in (**e**) plotted as a function of time over the same time period. The shaded areas in (**e**) and (**f**) indicate ±1 standard error of the mean (s.e.m.).

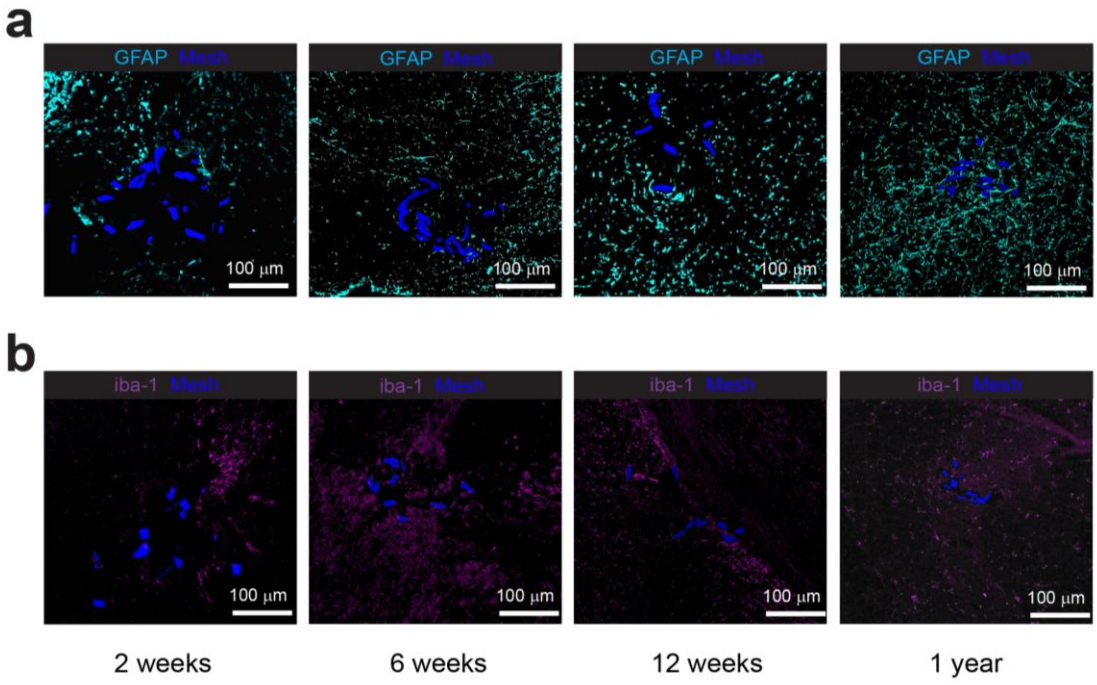

Supplementary Figure 7

Immunohistochemical images of horizontal sectioned mouse brains containing the mesh electronics from different times post-injection.

(**a**) GFAP stained images of representative horizontal brain slices used for normalized fluorescence intensity plots (**Fig. 2e**) showing the interfaces between mesh electronics and astrocytes, and (**b**) iba-1 stained images of representative horizontal slices used for normalized fluorescence intensity plots (**Fig. 2e**) showing the interfaces between mesh electronics and microglia at 2, 6 and 12 weeks post-injection. All samples were 10 μm-thick. Blue, cyan and purple correspond to mesh electronics, GFAP and iba-1, respectively. Scale bars: 100 μm.

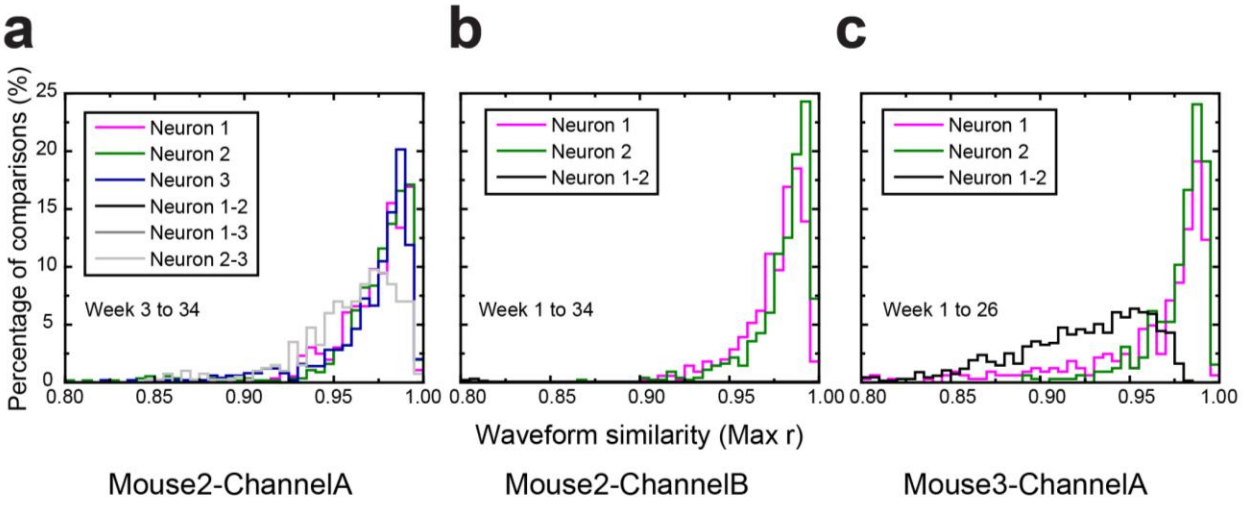

Supplementary Figure 8

Autocorrelation and cross-correlation analyses of average spike waveforms across all recording time points.

(**a**) Auto- and cross-correlation histograms for three identified neurons of Mouse2-ChannelA from week 3 to 34 post-injection shown in **Fig. 3b**. (**b**) Auto- and cross-correlation histograms for two identified neurons of Mouse2-ChannelB from week 1 to 34 post-injection shown in **Supplementary Fig. 10c**. (**c**) Auto- and cross-correlation histograms for two identified neurons of Mouse3-ChannelA from week 1 to 26 post-injection shown in **Supplementary Fig. 10d**.

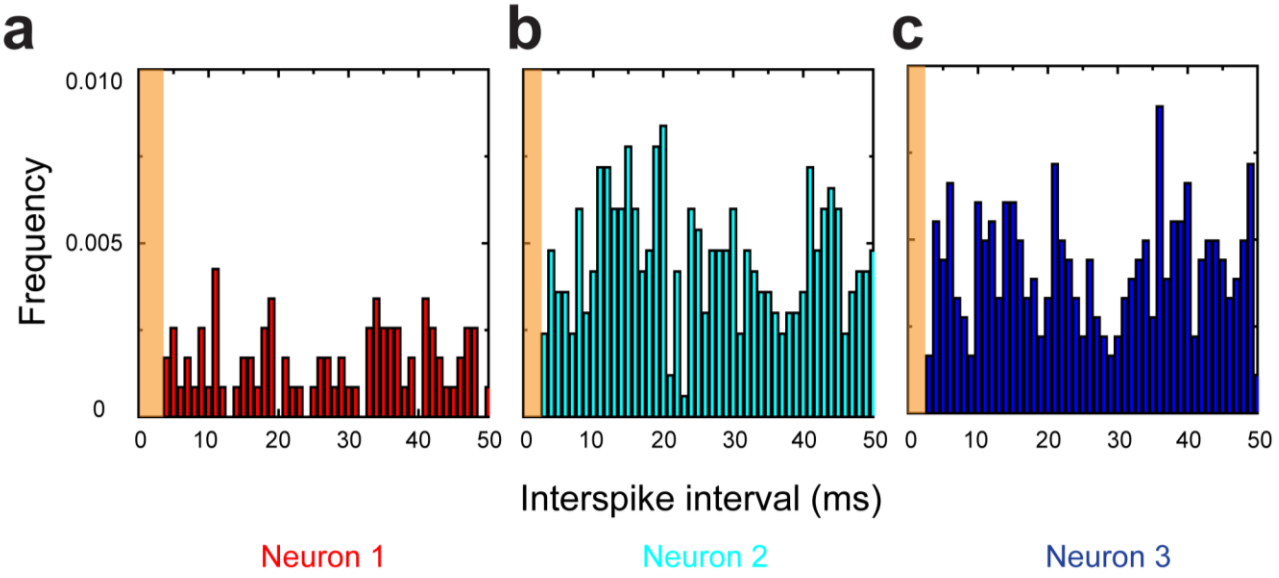

Supplementary Figure 9

Refractory periods of neuron firing.

(**a**-**c**) Interspike interval (ISI) histograms of the data shown in **Fig. 3c** at 26 weeks post-injection but replotted with a bin size of 1 ms. The data show clearly a 2-3 ms refractory period (orange-shaded regions) for neuron 1 (**a**), neuron 2 (**b**) and neuron 3 (**c**).

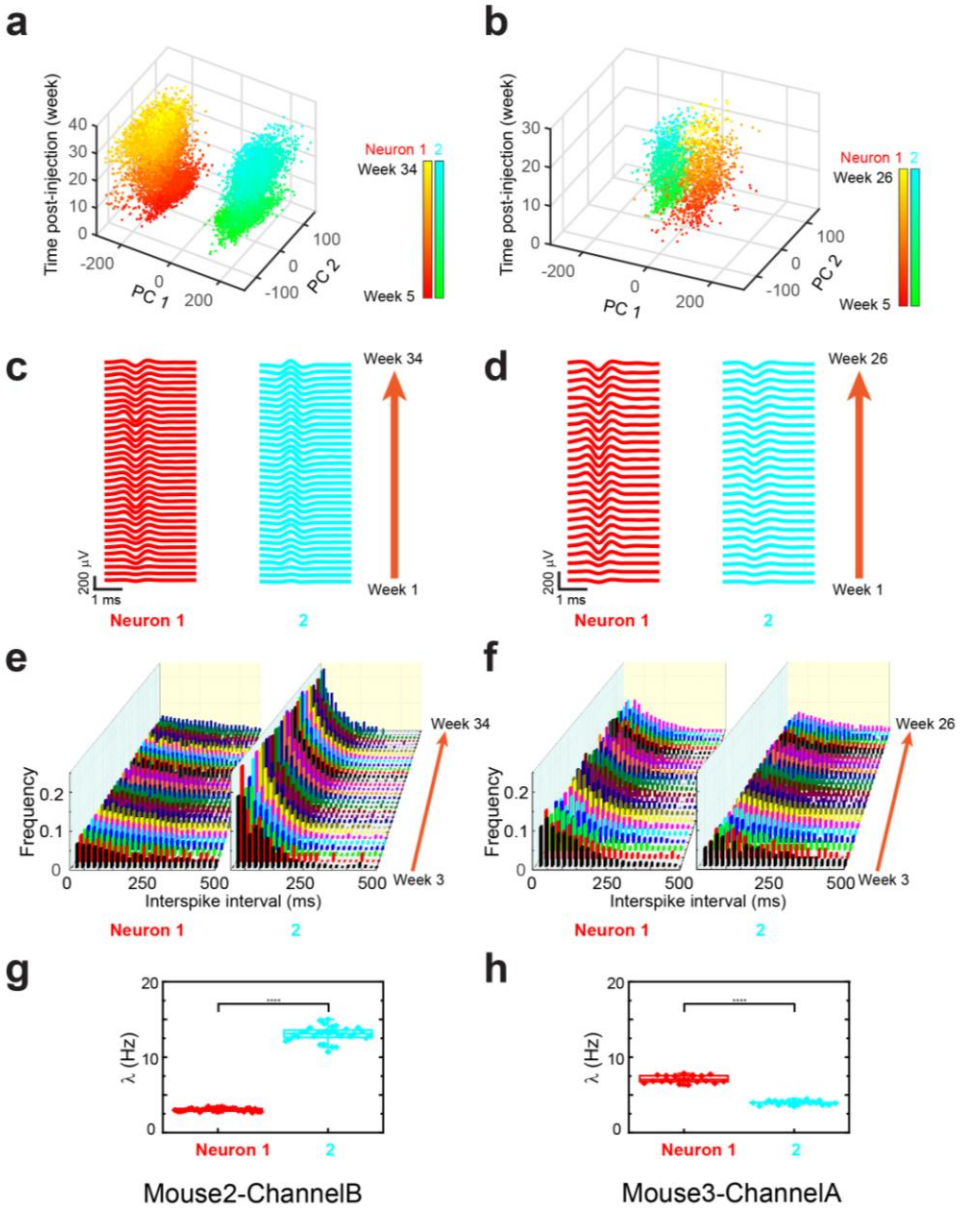

Supplementary Figure 10

Consistent tracking of the same group of neurons.

(**a**,**b**) Time evolution of representative single-unit spikes of Mouse2-ChannelB (**a**) and Mouse3-ChannelA (**b**) shown in **Fig. 2** clustered by principal component analysis (PCA) over eight and six months, respectively. In each plot, the x- and y-axis denote the first and second principal component, respectively, and the z-axis indicates post-injection time. (**c**,**d**) Time course analysis of average spike waveforms from each PCA cluster shown in (**a**) from 1 to 34 weeks post-injection (**c**), and for each PCA cluster shown in (**b**) from 1 to 26 weeks (**d**), respectively. (**e**,**f**) Time evolution of ISI histograms of each of the 2 neurons identified from the PCA clusters in (**a**) and (**b**) from 3 to 34 (**e**) and 3 to 26 weeks (**f**), respectively. Bin size: 20 ms. (**g**,**h**) Scatter plot with analysis of variance (ANOVA) (n=32 and 26 for (**g**) and (**h**), respectively) of the firing parameter, λ, obtained by fitting each ISI distribution profile shown in (**e**) and (**f**) to an exponential decay. All plots for Mouse3 are shown up to 26 weeks post-injection instead of 34 weeks shown for Mouse2, because Mouse3 was older than Mouse2 when the initial mesh electronics injection was carried out, and thus exhibited ageing-associated changes (shown in **Fig. 5** and **Supplementary Fig. 12**) at an earlier post-injection time point.

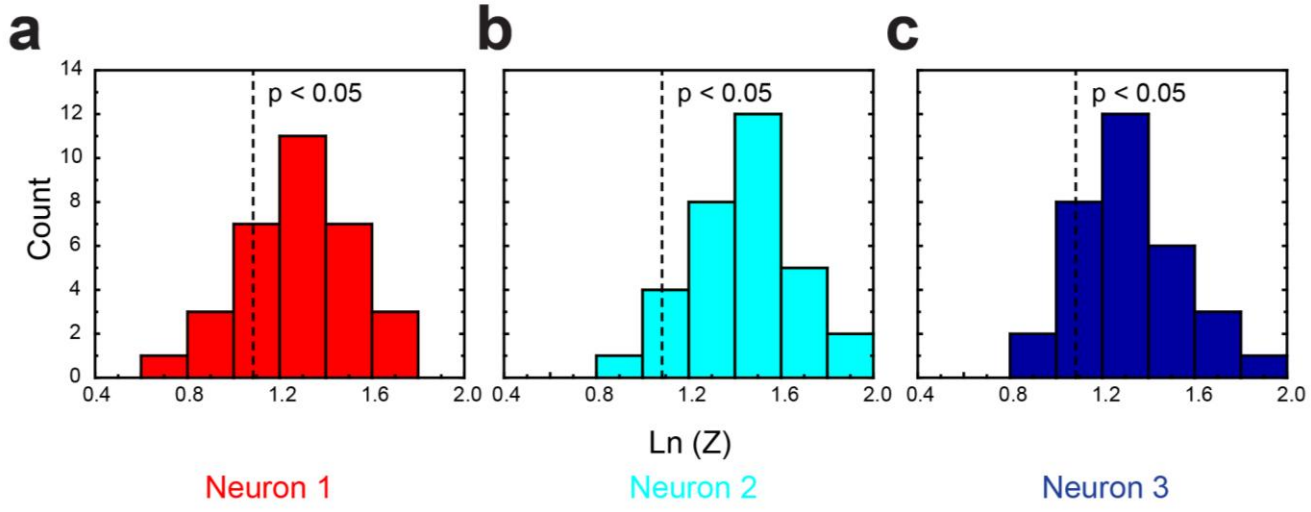

Supplementary Figure 11

Rayleigh Z-test of neuron phase-locking behavior.

(**a**-**c**) Rayleigh Z-test of all recording data for neuron 1 (**a**), neuron 2 (**b**) and neuron 3 (**c**) identified for Mouse2-ChannelA from week 3 to 34 post-injection (n=32). Each trial presents the recording data at a given week. The null hypothesis is: a given neuron does not have phase-locking behavior at a given week. The majority of trials on the right side of the vertical dashed lines suggest a >95% confidence interval ($p<0.05$) to reject the null hypothesis.

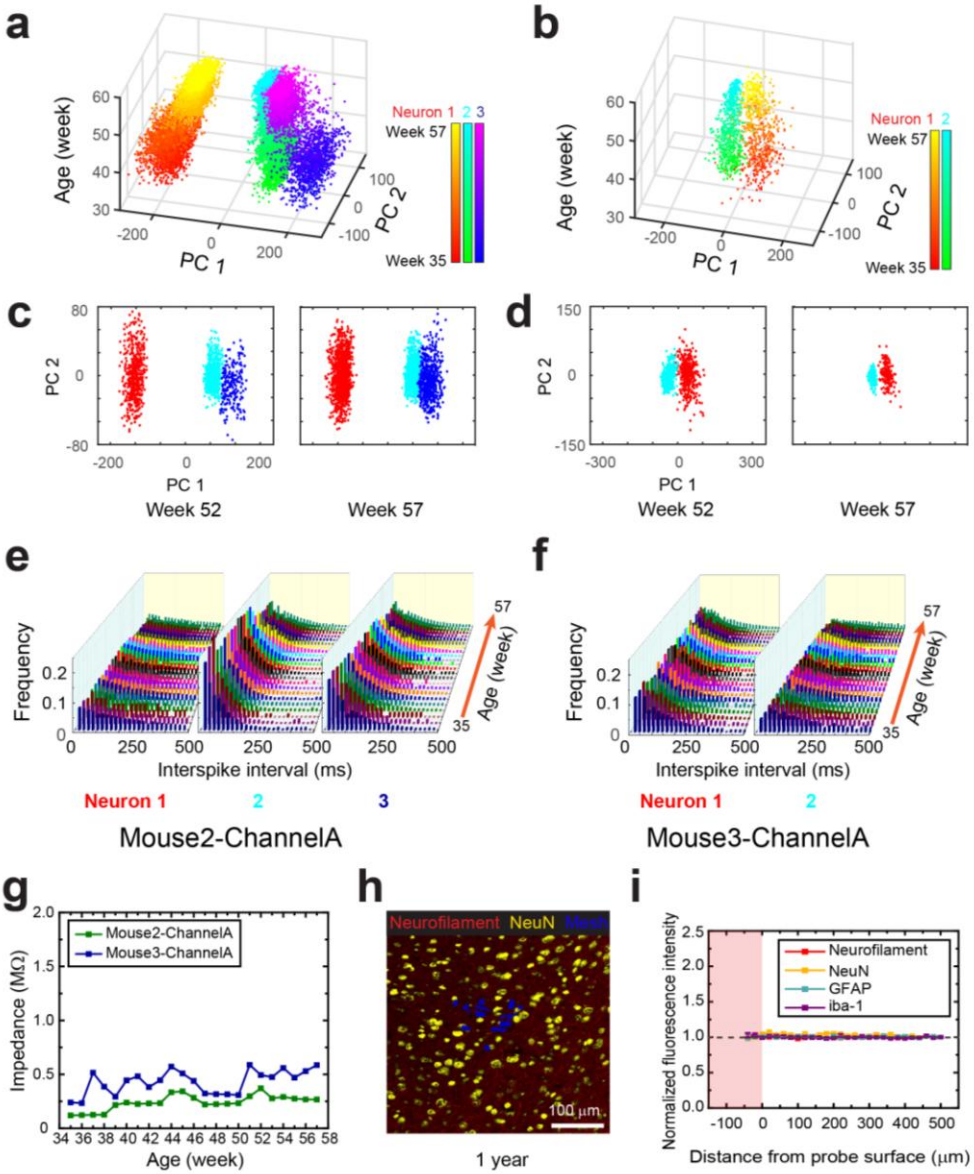

Supplementary Figure 12

Tracking of the same individual neurons during brain ageing.

(**a**,**b**) Time evolution of representative single-unit spikes of Mouse2-ChannelA (**a**) and Mouse3-ChannelA (**b**) shown in **Fig. 2** clustered by PCA from 35 to 57 weeks of age. In each plot, the x- and y-axes denote the first and second principal components, respectively, and the z-axis indicates the corresponding mouse age. (**c,d**) Representative 2D (PC1-PC2 plane) plots of the PCA results shown in (**a,b**) at week 52 and 57 of mouse age. (**e**,**f**) Time evolution of ISI histograms of each of the neurons identified from the PCA clusters in (**a**) and (**b**) from 35 to 57 weeks of age. Bin size: 20 ms. (**g**) Impedance values at 1 kHz of the two channels shown in (**a-f**) plotted as a function of mouse age over the same period. (**h**) Immunohistochemical images of a 10 μm-thick horizontal CTX brain slice showing the mesh electronics/brain tissue interface at 1-year mouse age. Red, yellow and blue colors correspond to neurofilaments, NeuN and mesh electronics, respectively. Scale bar: 100 μm. (**i**) Neurofilament (red), NeuN (yellow), GFAP (cyan) and iba-1 (purple) fluorescence intensity normalized against background values (gray dashed horizontal lines) plotted versus distance from the interface (see Online Methods). The pink-shaded regions indicate the interior of the mesh electronics. All error bars in this figure reflect ±1 standard error of the mean (s.e.m.).

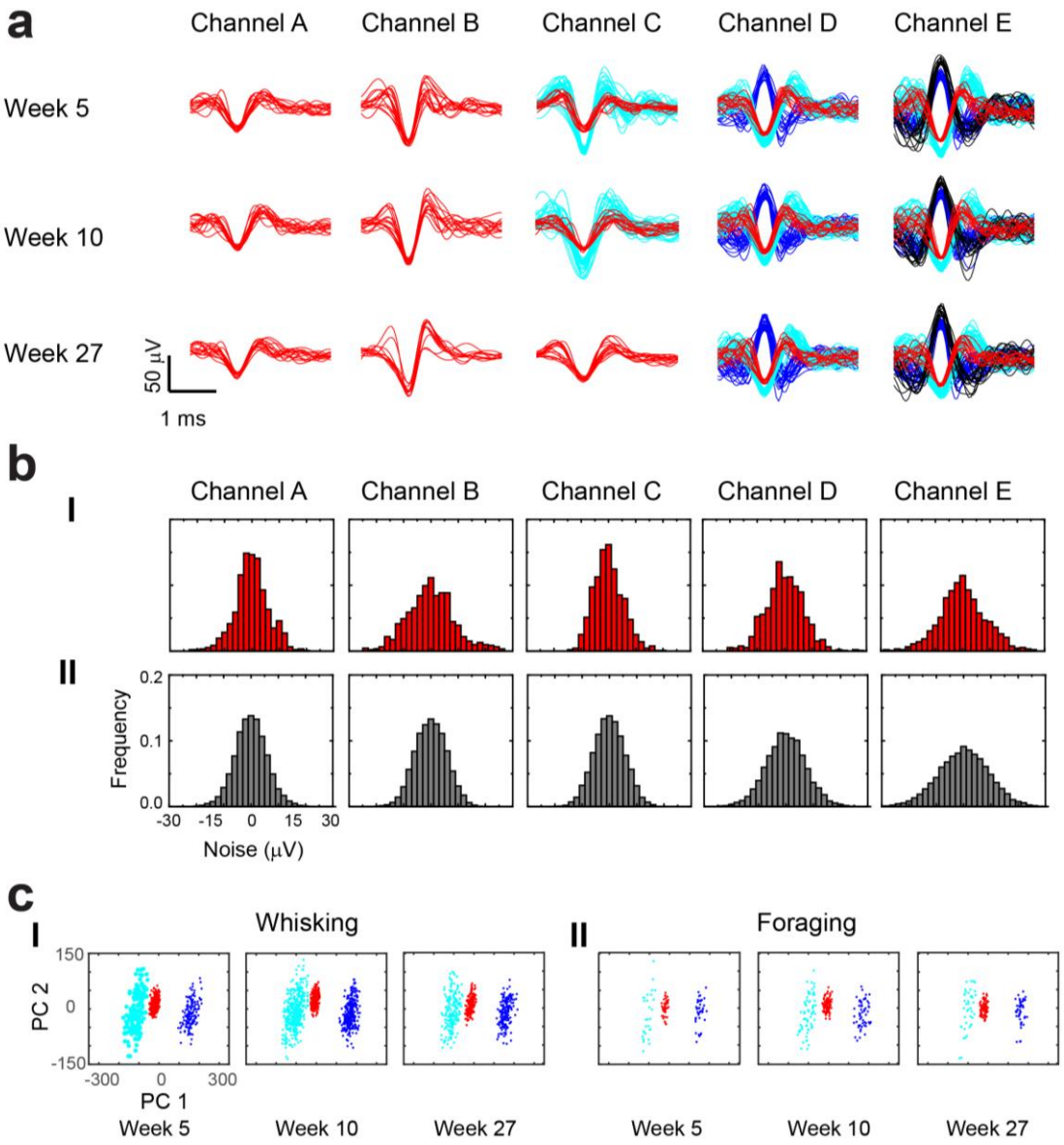

Supplementary Figure 13

Spike recordings from a freely behaving mouse.

(**a**) Sorted single-unit action potentials from chronic freely behaving mouse recordings. Each column represents the sorted spikes from an individual channel shown in **Fig. 6** at 5, 10 and 27 weeks post-injection. (**b**) Noise distributions of all red unit clusters of Channels A-E shown at week 10 in **a** (**I**), and the intrinsic recording noise of each corresponding electrode of the channel at the same week (**II**). See Online Methods for details of noise calculations. (**c**) Single-unit spikes of Channel D in (**a**) clustered by PCA when the mouse was actively whisking (**I**) and foraging (**II**) at week 5, 10 and 27.

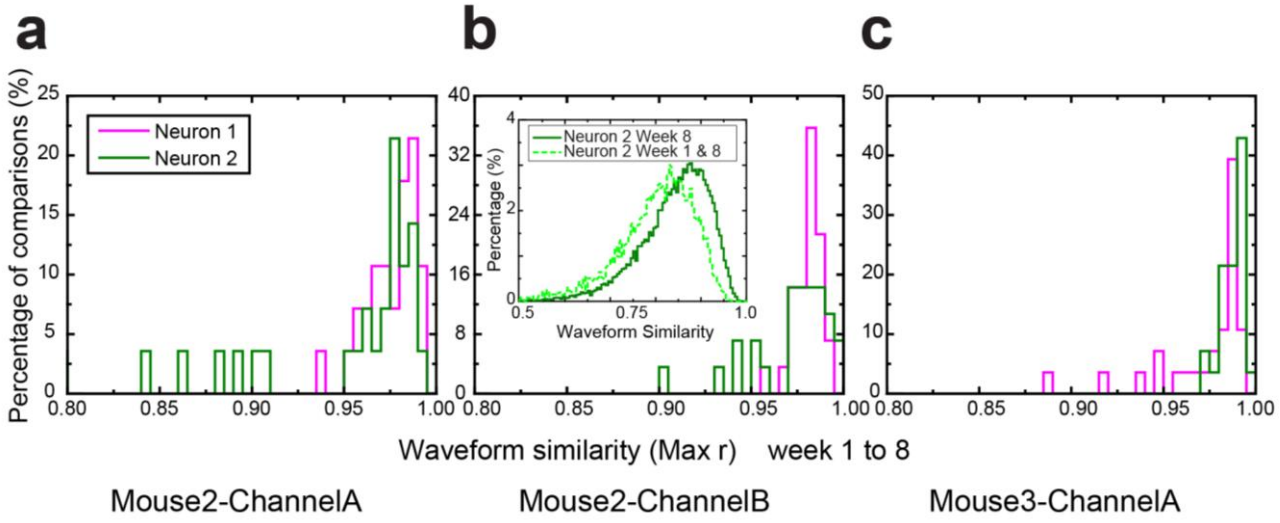

Supplementary Figure 14

Autocorrelation analyses of average waveforms from week 1 to 8 post-injection.

(**a**) Autocorrelation histograms of average waveforms for neurons 1 (magenta) and 2 (green) for Mouse2-ChannelA from weeks 1 to 8 post-injection shown in **Fig. 3b**. (**b**) Autocorrelation histograms of average waveforms for neurons 1 (magenta) and 2 (green) for Mouse2-ChannelB from weeks 1 to 8 shown in **Supplementary Fig. 10c**. Inset: Cross-correlation histogram of all raw spikes for neuron 2 between weeks 1 and 8 (light green, dashed line) and autocorrelation histogram of all raw spikes for neuron 2 on week 8 only (dark green, solid line). (**c**) Autocorrelation histograms of average waveforms for neurons 1 (magenta) and 2 (green) for Mouse3-ChannelA from weeks 1 to 8 shown in **Supplementary Fig. 10d**. See Online Methods for details of autocorrelation calculations.

Supplementary Information for:

Stable long-term chronic brain mapping at the single neuron level

Tian-Ming Fu, Guosong Hong, Tao Zhou, Thomas G. Schuhmann, Robert D. Viveros, and Charles M. Lieber*

*Corresponding author. E-mail: cml@cmliris.harvard.edu

This file includes:

Supplementary Tables 1-3

Nature Methods: doi:10.1038/nmeth.3969

Supplementary Table 1. L_{ratio} calculated with the same degree of freedom (df) of eight for each identified neuron in Mouse2-ChannelA, Mouse2-ChannelB and Mouse3-ChannelA at 2, 4 and 6 months post-injection. An $L_{ratio}<0.05$ for a specific isolated unit among all sorted spikes is considered good separation/isolation as discussed previously[36,49]. See Online Methods for details of L_{ratio} calculations.

	Mouse2-ChannelA Neuron1	Mouse2-ChannelA Neuron2	Mouse2-ChannelA Neuron3	Mouse2-ChannelB Neuron1	Mouse2-ChannelB Neuron2	Mouse3-ChannelA Neuron1	Mouse3-ChannelA Neuron2
2 months	2.7×10^{-5}	2.2×10^{-3}	1.9×10^{-3}	4.2×10^{-4}	2.4×10^{-5}	3.2×10^{-3}	1.7×10^{-3}
4 months	3.1×10^{-5}	2.0×10^{-3}	4.7×10^{-3}	7.2×10^{-4}	6.6×10^{-5}	4.3×10^{-3}	3.6×10^{-3}
6 months	4.0×10^{-6}	1.1×10^{-3}	5.5×10^{-3}	4.2×10^{-4}	1.4×10^{-4}	1.8×10^{-2}	9.9×10^{-3}

Supplementary Table 2. Rayleigh Z-test of locked-phase alteration for each neuron shown in **Supplementary Fig. 11**. The null hypothesis is: The locked phase of a specific neuron has a random distribution through time evolution. A Ln(Z) value of >1.09 (i.e., Z>2.97) (sample size n=32) can reject the null hypothesis with a confidence interval >95% (p value of <0.05)[39]. See Online Methods for details of Rayleigh Z-test.

	Neuron 1	Neuron 2	Neuron 3
Z-value	27.85	27.76	24.95
Ln(Z)	3.33	3.32	3.22

Supplementary Table 3. Standard deviation of noise distribution within an entire recording session of all sorted spike clusters at week 10 post-injection shown in **Supplementary Fig. 13a**, and comparisons with intrinsic recording noise of each channel. Colors in column-1 correspond to the color-coded spike clusters in **Supplementary Fig. 13a**. See Online Methods for details of standard deviation extraction.

Standard deviation of noise distribution (μV)	Channel A	Channel B	Channel C	Channel D	Channel E
Red	4.95	7.52	5.20	6.51	7.23
Cyan	NA	NA	10.79	7.83	9.13
Blue	NA	NA	NA	8.49	9.27
Black	NA	NA	NA	NA	9.42
Intrinsic recording noise	5.58	5.98	5.79	7.00	9.10

Nature Methods: doi:10.1038/nmeth.3969